

ACTIVE GALACTIC NUCLEI EMISSION-LINE PROPERTIES VERSUS EDDINGTON RATIO

CRAIG WARNER¹, FRED HAMANN¹, AND MATTHIAS DIETRICH²
Draft version December 4, 2018

ABSTRACT

We analyze UV spectra for a large sample of 578 Type 1 Active Galactic Nuclei and derive Eddington ratios, L/L_{edd} , from the bolometric luminosities and emission line widths for each object in the sample. The sample spans five orders of magnitude in supermassive black hole (SMBH) mass, seven orders of magnitude in luminosity, and a redshift range from $0 \leq z \leq 5$. We include a sample of 26 low-redshift Narrow-Line Seyfert 1s (NLS1s) for comparative analysis. The NLS1s have slightly larger than average L/L_{edd} ratios (and smaller SMBH masses) for their luminosities, but those L/L_{edd} values are still substantially below the average for luminous quasars. A large fraction (27%) of the objects overall have $L/L_{\text{edd}} > 1$, which might be explained by non-spherically symmetric accretion. We find no trend between L/L_{edd} and either redshift or SMBH mass. Composite spectra sorted by L/L_{edd} show an unusual emission-line behavior: nearly constant peak heights and decreasing FWHMs with increasing L/L_{edd} . This is in marked contrast to the emission-line behaviors with luminosity, SMBH mass, and FWHM(C IV), which clearly show trends analogous to the Baldwin Effect: decreasing line peaks and equivalent widths with increasing luminosity, SMBH mass, and FWHM. The origins of the unusual behavior with L/L_{edd} are not understood, but one implication is that metallicity estimates based on emission line ratios involving nitrogen show no trend with L/L_{edd} in the composite spectra created from different ranges in L/L_{edd} . The NLS1 composite, however, shows a slightly high metallicity for its SMBH mass and luminosity. Our earlier work suggests that host galaxy mass, correlated with SMBH mass and AGN luminosity, is the fundamental parameter affecting BLR metallicities. Some secondary effect, not related to L/L_{edd} , must be enhancing the metallicities in NLS1s.

Subject headings: galaxies: active—quasars: emission lines—galaxies: formation

1. INTRODUCTION

The central engines of quasars, and more generally, active galactic nuclei (AGNs) are believed to be powered by supermassive black holes (SMBHs). Two of the fundamental properties of AGNs are the SMBH mass and the accretion rate of material onto the SMBH. Several indirect methods have been devised to estimate SMBH masses. One set of these methods assumes that the broad emission-line region (BLR) is in gravitational equilibrium with the central source, so that the SMBH mass can be estimated by applying the virial theorem, $M_{\text{SMBH}} = rv^2/G$, to the measured line widths (Peterson 1993; Peterson 1997; Wandel et al. 1999; Kaspi et al. 2000; McLure & Dunlop 2001; Vestergaard 2002). In reverberation mapping studies, R_{BLR} , the radial distance between the central source and the BLR can be estimated from the lag time between continuum variations and the emission-line response (Peterson 1993; Peterson 1997; Wandel et al. 1999; Kaspi et al. 2000). These reverberation mapping studies have demonstrated an observed relation of $R_{\text{BLR}} \propto \lambda L_{\lambda}(5100 \text{ \AA})^{0.7}$ that can be used to estimate R_{BLR} for AGNs over a wide range of redshifts (Kaspi et al. 2000; McLure & Dunlop 2001; Vestergaard 2002; Corbett et al. 2003; Warner et al. 2003). Netzer (2003) has argued that the slope is not known to an accuracy better than about 0.15.

A second set of methods is based on the tight correlation between the masses of SMBHs and the velocity dispersions, σ , of their host galaxy spheroidal components

(Ferrarese & Merritt 2000; Gebhardt et al. 2000; Merritt & Ferrarese 2001; Tremaine et al. 2002). However, stellar velocity dispersions are not easy to measure for AGN hosts, especially at high redshifts. Because of this, methods have been devised using proxies of the velocity dispersion, such as the width of the narrow emission line [O III] $\lambda 5007$ (Nelson 2000; Boroson 2003; Shields et al. 2003) or the bulge luminosity, L_{bulge} (Magorrian et al. 1998; Laor 1998; Wandel 1999). Early studies showed a large scatter, as much as two orders of magnitude between SMBH mass and L_{bulge} (Ferrarese & Merritt 2000). However, more recent studies that carefully model the bulge light profiles of disk galaxies and thus obtain more accurate values of L_{bulge} show less scatter in $M_{\text{SMBH}} - L_{\text{bulge}}$, similar to that in the $M_{\text{SMBH}} - \sigma$ relationship (McLure & Dunlop 2002; Erwin et al. 2002; Bettoni et al. 2003). Recently, SMBH mass has also been shown to correlate strongly with the global structure of bulges and ellipticals, such that more centrally concentrated bulges have more massive SMBHs. This relationship is as strong as the $M_{\text{SMBH}} - \sigma$ relationship with comparable scatter (Graham et al. 2001; Erwin et al. 2002).

Once the SMBH mass has been estimated, the Eddington luminosity can be calculated as $L_{\text{edd}} = 1.26 \times 10^{38} M_{\text{SMBH}} (M_{\odot}) \text{ ergs s}^{-1}$ (e.g., Rees 1984; Peterson 1997). Eddington luminosity is the limit in which the inward gravitational force acting on the gas exactly balances the outward radiation force induced by electron scattering. It can be thought of as the maximum possible luminosity

¹ Department of Astronomy, University of Florida, 211 Bryant Space Science Center, Gainesville, FL 32611-2055, E-mail: warner@astro.ufl.edu, hamann@astro.ufl.edu

² Department of Physics and Astronomy, Georgia State University, Atlanta, Georgia 30303

for an object of mass M_{SMBH} that is powered by *spherical* accretion (Peterson 1997). The Eddington luminosity can be exceeded if accretion is not spherically symmetric (see §5, also Osterbrock 1989; Begelman 2002; Collin et al. 2002; Wang 2003). AGN luminosities should be directly proportional to the accretion rate, $L \propto \dot{M}_{\text{acc}}$, and therefore the ratio, $L/L_{\text{Edd}} \propto \dot{M}_{\text{acc}}/M$, is an indirect measure of the accretion rate relative to the critical Eddington value.

Narrow Line Seyfert 1s (NLS1s) are a subclass of Seyfert 1s that exhibit distinct and unusual properties: very narrow broad emission lines ($H\beta$ FWHM $< 2000 \text{ km s}^{-1}$) with [O III] $\lambda 5007 / H\beta$ ratios of less than 3 (to exclude Seyfert 2s), strong Fe II emission, and unusually strong big blue bumps (Osterbrock & Pogge 1985; Kuraszkiewicz et al. 2000; Constantin & Shields 2003). NLS1s also land at one extreme end of the Boroson & Green (1992) Principal Component 1 (PC1). It has been suggested that PC1 is strongly correlated with L/L_{Edd} (Boroson & Green 1992; Boroson 2002; Shemmer & Netzer 2002; Constantin & Shields 2003). Several studies have suggested that NLS1s have low SMBH masses for their luminosities, and thus very high Eddington ratios, near 1 (Mathur 2000; Kuraszkiewicz et al. 2000; Shemmer & Netzer 2002; Shemmer et al. 2003). It has also been suggested that NLS1s have unusually high metallicities for their luminosities (see §4.4 and Figure 11 below, Mathur 2000; Shemmer & Netzer 2002; Shemmer et al. 2003). Shemmer & Netzer (2002) find that NLS1s depart from the nominal relationship between metallicity and luminosity in AGNs (Hamann & Ferland 1999; Dietrich et al. 2003, in prep), with some NLS1s indicating metallicities as high as those measured in high-luminosity, high-redshift quasars. Because of their high metallicities and high Eddington ratios, Mathur (2000) proposed that NLS1s are analogs of high-redshift ($z \gtrsim 4$) quasars, in that they may both be in an early evolutionary phase, residing in young host galaxies.

We have collected a large sample of 578 spectra of “Type 1” AGNs (quasars and Seyfert galaxies with broad emission lines) that span the rest-frame UV wavelengths needed for this study (Dietrich et al. 2002). We compute composite spectra from different ranges in the Eddington ratio, L/L_{Edd} . We include a composite spectrum produced from a subsample of 26 NLS1s for comparative analysis. We present measurements of the emission lines in these composite spectra and investigate their relationship to L/L_{Edd} .

2. EDDINGTON RATIO DETERMINATIONS

We first estimate SMBH masses by applying the virial theorem, $M_{\text{SMBH}} = rv^2/G$, to the line-emitting gas (for more details, see also Kaspi et al. 2000; Peterson & Wandel 2000; McLure & Dunlop 2001; Vestergaard 2002; Corbett et al. 2003; Warner et al. 2003). Kaspi et al. (2000) express the SMBH mass as

$$M_{\text{SMBH}} = 1.5 \times 10^5 M_{\odot} \left(\frac{R_{\text{BLR}}}{\text{lt - days}} \right) \left(\frac{\text{FWHM}}{10^3 \text{ km s}^{-1}} \right)^2 \quad (1)$$

R_{BLR} is the radial distance between the BLR and the central source, and FWHM applies to the broad emission line profile. We estimate R_{BLR} based on the observed relation between R_{BLR} for a particular line and the continuum luminosity (Wandel et al. 1999; Kaspi et al. 2000; Vestergaard 2002; Corbett et al. 2003). A particular line must be specified because reverberation studies have shown that the BLR is radially stratified, such that higher ionization lines tend to form closer to the central engine than lower ionization lines (Peterson 1993).

We select the C IV $\lambda 1549$ emission line instead of $H\beta$ to estimate SMBH masses because it is more readily observed across the entire redshift range from $z \sim 0$ to $z \sim 5$. We find that there is approximately a 1:1 correlation between the SMBH mass obtained from C IV and that obtained from $H\beta$. There can be significant deviations from this for individual objects, but the relation holds well for averages of many objects and for measurements based on composite spectra (see Vestergaard 2002; Warner et al. 2003 for further discussion).

Reverberation studies indicate that the radius of the BLR for C IV is about half that of $H\beta$ (Stirpe et al. 1994; Korista et al. 1995; Peterson 1997; Peterson & Wandel 1999). We therefore modify the equation given by Kaspi et al. (2000) to obtain

$$R_{\text{BLR}}(\text{CIV}) = 9.7 \left[\frac{\lambda L_{\lambda}(1450\text{\AA})}{10^{44} \text{ ergs s}^{-1}} \right]^{0.7} \text{ lt - days} \quad (2)$$

See Warner et al. (2003) for more details. From Equations (1) and (2), we derive

$$M_{\text{SMBH}} = 1.4 \times 10^6 M_{\odot} \left(\frac{\text{FWHM}(\text{CIV})}{10^3 \text{ km s}^{-1}} \right)^2 \left(\frac{\lambda L_{\lambda}(1450\text{\AA})}{10^{44} \text{ ergs s}^{-1}} \right)^{0.7} \quad (3)$$

Vestergaard (2002) calibrated mass derivations based on C IV against estimates using $\text{FWHM}(H\beta)$ and direct measurements of $R_{\text{BLR}}(H\beta)$ from reverberation mapping. Her technique yields essentially the same mass relationship (within 10%) as Equation 3, which helps to confirm the factor of 2 scaling adopted here between $R_{\text{BLR}}(\text{C IV})$ and $R_{\text{BLR}}(H\beta)$. Vestergaard (2002) finds that SMBH masses estimated by applying this equation to single-epoch spectra of individual objects have a 1σ uncertainty of a factor of three when compared to studies that use $H\beta$ and a direct, reverberation measure of the BLR radius. Our composite spectra average over variabilities and object-to-object scatter, which should significantly reduce the uncertainties. See also Krolik (2001), Netzer (2003), Corbett et al. (2003), and Vestergaard (2004) for further discussion of the uncertainties.

We next estimate bolometric luminosities, L , based on an integration over a typical quasar continuum shape. We use the cosmological parameters $H_0 = 65 \text{ km s}^{-1} \text{ Mpc}^{-1}$, $\Omega_M = 0.3$, and $\Omega_{\Lambda} = 0$ (Carroll, Press, & Turner 1992) throughout this paper³. We assume a segmented power-law of the form $F_{\nu} \propto \nu^{\alpha}$ to approximate the continuum shape, with $\alpha = -0.9$ from 0.1 \AA to 10 \AA , $\alpha = -1.6$ from 10 \AA to 1000 \AA , and $\alpha = -0.4$ from 1000 \AA to $100,000 \text{ \AA}$ (Zheng et al. 1997; Laor et al. 1997; Brotherton et al. 2001; Vanden Berk et al. 2001; Dietrich et al. 2002). It

³ The use of this cosmology was motivated for comparison with earlier studies in the pre-WMAP era. Furthermore, the difference between our set of cosmological parameters and those suggested by WMAP results in a difference of less than 20% in luminosity for a wide redshift range of $0 < z < 4$.

is now well established that the mean UV–IR slope is a function of luminosity (see Dietrich et al. 2002). For the luminosity range spanned by our sample, the average powerlaw index between 1000 Å and 100,000 Å ranges from ~ -0.2 to ~ -0.6 (M. Dietrich, private communication). This range could cause a scatter of $\sim 20\%$ in our estimates of L .

Integrating this nominal spectrum over all wavelengths implies bolometric corrections of 4.36 and 9.27 for $\lambda L_\lambda(1450\text{Å})$ and $\lambda L_\lambda(5100\text{Å})$, respectively. These corrections are slightly lower than the correction of 11.8 to $\lambda L_\lambda(5100\text{Å})$ derived by Elvis et al. (1994), but in good agreement with more recent derivations (Kaspi et al. 2000; Vestergaard 2004). We use this bolometric correction and SMBH masses from Equation (3) to obtain Eddington ratios:

$$\frac{L}{L_{\text{edd}}} = 1.6 \left(\frac{\text{FWHM(CIV)}}{10^3 \text{ km s}^{-1}} \right)^{-2} \left(\frac{L}{10^{44} \text{ ergs s}^{-1}} \right)^{0.3} \quad (4)$$

3. DATA & ANALYSIS

Our sample is comprised of 578 Type 1 (broad-line) AGN spectra with rest-frame UV wavelength coverage that encompasses the range $950 \lesssim \lambda \lesssim 2050$ Å. The spectra were obtained by several groups using various ground-based instruments as well as the *Hubble Space Telescope* (*HST*) and the *International Ultraviolet Explorer* (*IUE*) (see Dietrich et al. 2002 and 2004, in prep for more details). The sample spans a redshift range from $0 \lesssim z \lesssim 5$, seven orders of magnitude in luminosity, and five orders of magnitude in SMBH mass. One unique aspect of this sample is that it contains new observations of faint quasars at redshift $z > 2.5$ (e.g., Steidel et al. 2002, Dietrich et al. 2002). Thus we can avoid to some degree the bias toward higher luminosities at higher redshifts inherent in magnitude-limited samples. The sample spans at least three orders of magnitude in luminosity at all redshifts (see Fig. 1 in Dietrich et al. 2002). We determined the radio loudness for the quasars using the radio flux densities given in Véron-Cetty & Véron (2001). We used the definition of radio loudness given by Kellermann et al. (1989). Our classifications of radio-loud quasars are consistent with classifications available in the literature (Wills et al. 1995; Bischof & Becker 1997; Wilkes et al. 1999; Stern et al. 2000).

We use an automated program to estimate the FWHM of C IV in each spectrum (see Warner et al. 2003 for details). Comparisons between the FWHMs estimated by the program and those measured manually indicate an error of $\lesssim 10\%$ in the automated results. Lines containing significant absorption are flagged by the program and their FWHMs are estimated manually (by interpolating across the absorption feature). We use the FWHM of C IV and the continuum luminosity, $\lambda L_\lambda(1450\text{Å})$ to estimate the central SMBH mass and L/L_{edd} for each quasar based on the equations given in §2.

We then sort the quasars by L/L_{edd} into seven bins (see Figure 1): $L/L_{\text{edd}} < 0.25$, $0.25 \leq L/L_{\text{edd}} < 0.33$, $0.33 \leq L/L_{\text{edd}} < 0.50$, $0.50 \leq L/L_{\text{edd}} < 0.67$, $0.67 \leq L/L_{\text{edd}} < 1.00$, $1.00 \leq L/L_{\text{edd}} < 2.00$, and $L/L_{\text{edd}} \geq 2.00$, and compute seven composite spectra. Each composite spectrum is the average of all the quasar spectra in a bin. Table 1 lists various parameters for the composites, includ-

ing the mean values of M_{SMBH} , L , FWHM(C IV) , L/L_{edd} , and the redshift, z , as measured from the individual objects contributing to each composite. Also listed are the numbers of objects contributing at the wavelength of the C IV emission line. The spectral slopes, α , are measured from each composite spectrum and constrained by the flux in 20 Å wide windows centered at 1450 Å and 1990 Å.

Calculating composite spectra significantly improves the signal-to-noise ratio and averages over object-to-object variations. Since narrow absorption features may affect the emission line profiles in composite spectra, we developed a method to detect strong narrow absorption features. The contaminated spectral region of the individual spectrum is then excluded from the calculation of the composite spectrum. For more details about creating composite spectra, see Brotherton et al. (2001), Vanden Berk et al. (2001), Dietrich et al. (2002), and Warner et al. (2003).

For comparison with the L/L_{edd} composites, we also create composite spectra for different ranges in SMBH mass ($10^6 - 10^7 M_\odot$, $10^7 - 10^8 M_\odot$, $10^8 - 10^9 M_\odot$, $10^9 - 10^{10} M_\odot$, and $\geq 10^{10} M_\odot$; see also Warner et al. 2003), L ($10^{44} - 10^{45}$ ergs s^{-1} , $10^{45} - 10^{46}$ ergs s^{-1} , $10^{46} - 10^{47}$ ergs s^{-1} , $10^{47} - 10^{48}$ ergs s^{-1} , and $10^{48} - 10^{49}$ ergs s^{-1}), and FWHM(C IV) (< 2000 km s^{-1} , $2000 - 4000$ km s^{-1} , $4000 - 6000$ km s^{-1} , $6000 - 8000$ km s^{-1} , and ≥ 8000 km s^{-1}). See Table 1 for additional information.

We also create a composite spectrum of 26 NLS1s that were classified by others according to the criteria described in §1 (Kuraszkiewicz et al. 2000; Wang & Lu 2001; Constantin & Shields 2003). This subsample is drawn from the same overall sample used to create the other composites described above. Eighteen of these objects have data at C IV and they span a range in L/L_{edd} from ~ 0.1 to 2.

We correct each composite spectrum for strong iron emission lines using the empirical Fe emission template that was extracted from I Zw 1 by Vestergaard & Wilkes (2001), which they very kindly provided for this study (see Dietrich et al. 2002 and Warner et al. 2003 for more details). The Fe II contribution is generally small at wavelengths $\lesssim 2000$ Å, but the correction for this emission improves the measurements of weak lines such as N III] $\lambda 1750$ and He II $\lambda 1640$. We fit the continuum of each Fe-subtracted spectrum with a powerlaw of the form $F_\nu \propto \nu^\alpha$. Figure 2 shows the final Fe II-subtracted composite spectra normalized by the continuum fits.

To measure the broad emission lines, we use a spectral fitting routine developed in the IDL language, that employs χ^2 minimization. We fit each line with one or more Gaussian profiles, with the goal of simply measuring the total line strengths free of blends. When necessary, we use the profile of strong unblended lines, such as C IV, to constrain the fits to weaker or more blended lines (see Warner et al. 2003 for details of our fitting procedure). Figure 3 shows an example of our fits.

The continuum location is the primary uncertainty in our flux measurements. We estimate the 1σ standard deviation of our measurements of the fluxes of Ly α and C IV to be $\lesssim 10\%$ based on repeated estimates with the continuum drawn at different levels. We estimate the uncertainty in weaker lines by the same method to be $\sim 10\text{--}20\%$. There are also secondary uncertainties due to line blending, which can be important for some of the weak lines

and for N V in the wing of Ly α .

4. RESULTS & COMPARISONS

4.1. L/L_{Edd} and Super-Eddington Accretion

Figure 4 shows the distribution of L/L_{Edd} for the entire sample. A large fraction (27%) of the objects in our sample have $L/L_{\text{Edd}} > 1$ (see also Fig. 1). This result is not precise because our mass estimates for individual objects have factor of ~ 3 uncertainties (§2), which are comparable to the width of the distribution in Figure 4. Nonetheless, it is interesting that the sample mean is close to the Eddington limit, with $\langle L/L_{\text{Edd}} \rangle \sim 0.9$ (Fig. 4). Also note that trends with L/L_{Edd} that we discuss below are more reliable than the individual measurements because they rely on relative L/L_{Edd} .

Consistent with previous studies (§1), we find that the NLS1s have generally high Eddington ratios for their luminosities, including several objects with $L/L_{\text{Edd}} \gtrsim 1$. However, the NLS1s do not have the highest Eddington ratios in our sample. Quasars with high luminosities and narrow C IV emission lines often have $L/L_{\text{Edd}} > 2$. The most extreme of these objects, such as BR2248-1242 (see Warner et al. 2002), can have derived Eddington ratios approaching 10 (see Figure 1).

4.2. Correlations with L/L_{Edd}

Figure 5 shows the distributions in redshift, bolometric luminosity, FWHM(C IV), and SMBH mass as a function of L/L_{Edd} for the entire sample. L/L_{Edd} correlates positively with L and negatively with FWHM(C IV), but these correlations may be attributed largely to our derivation of L/L_{Edd} from these quantities. In fact, the slopes in these correlations are matched well by the parameter relationships in Equation 4. In agreement with Woo & Urry (2002), we find no trend between L/L_{Edd} and either redshift or SMBH mass. We find that the weak trend in Figure 5 between L/L_{Edd} and redshift is due to i) a trend for larger L/L_{Edd} with increasing L , and ii) a bias for more high L objects at higher redshifts in our sample. Sub-samples spanning narrow ranges in luminosity show that there is no trend between L/L_{Edd} and redshift once these biases are removed (see Figure 6). In all four panels of Figure 5, there are no clear differences between radio loud and radio quiet objects.

Table 1 shows that there is no apparent trend between Eddington ratio and the slope of the UV continuum. The NLS1 composite, though, exhibits a steeper (softer) UV spectrum than the L/L_{Edd} composites (see Table 1). This is consistent with findings that NLS1s in general have redder spectra than typical Type 1 AGNs (e.g., Crenshaw et al. 2002; Constantin & Shields 2003).

Table 2 lists for each L/L_{Edd} and NLS1 composite spectrum the line fluxes relative to Ly α , the rest-frame equivalent widths (REWs) as measured above the fitted continuum, and the FWHMs. Figure 7 plots the REWs of selected emission lines as a function of L/L_{Edd} . The NLS1 composite spectrum is displayed (plotted as a triangle) for comparative purposes. The dotted lines are linear fits to the L/L_{Edd} composite data (excluding the NLS1 composite). Interestingly, while most emission lines decrease in REW with increasing L/L_{Edd} , Ly α and O VI exhibit a positive trend between REW and L/L_{Edd} , and N III]

shows no trend at all. O VI has larger measurement errors than most other emission lines, so it is unclear whether this positive trend between O VI REW and L/L_{Edd} is real or not.

The REWs of emission lines in the NLS1 composite (represented by a triangle) generally do not match the trend fit to the L/L_{Edd} composites in Figure 7. The NLS1 composite is above the fitted trend for some emission lines and below the fitted trend for others, regardless of the slopes of the trends.

4.3. Surprising Emission-Line Behaviors

The composite spectra sorted by L/L_{Edd} show a surprising emission-line behavior: nearly constant peak heights and decreasing FWHMs with increasing L/L_{Edd} (see Figure 2). This is in marked contrast to the emission-line behaviors in composite spectra sorted by luminosity, SMBH mass, and FWHM(C IV), which clearly show trends analogous to the Baldwin Effect: decreasing line peaks and equivalent widths with increasing luminosity, SMBH mass, and FWHM. Figure 8 compares the emission-line behaviors in these different composites (see also Wills et al. 1993; Croom et al. 2002; Dietrich et al. 2002; Warner et al. 2003). In particular, the composite spectra created from different ranges in FWHM(C IV) clearly show a trend analogous to the Baldwin Effect despite spanning a range of less than half an order of magnitude in average luminosity (Table 1). In contrast, the L/L_{Edd} composites span a wide range in FWHM(C IV) and an order of magnitude in average luminosity but do not show any behavior similar to the Baldwin Effect. This suggests that the Baldwin Effect may actually be related to SMBH mass (which correlates positively with both L and FWHM), since the L/L_{Edd} composites have nearly constant M_{SMBH} .

To illustrate this point further, Figure 9 compares L/L_{Edd} composite spectra created for a narrow range in SMBH mass ($10^8 M_{\odot} < M_{\text{SMBH}} < 10^9 M_{\odot}$) and a narrow luminosity range (10^{47} ergs/s $< L < 10^{48}$ ergs/s). Both sets of spectra are shown prior to normalization to the continuum. The emission line behavior described above (e.g. constant peak heights, etc.) is clearly evident in the L/L_{Edd} composites at nearly constant M_{SMBH} , but *not* in the composites with nearly constant L . The composites at nearly constant L show a trend for decreasing peak heights and equivalent widths with increasing M_{SMBH} .

In composite spectra sorted by luminosity, SMBH mass, and FWHM(C IV), the Baldwin Effect is not seen in N V (see Figure 8, also Dietrich et al. 2002; Warner et al. 2003), leading to a higher N V / C IV ratio in objects with higher luminosities, SMBH masses, and FWHMs(C IV). However, in the L/L_{Edd} composites created from our entire sample, N V clearly decreases in REW as L/L_{Edd} increases, yielding a nearly constant N V / C IV ratio across the full range of L/L_{Edd} (see Figure 10). Furthermore, the L/L_{Edd} composites created from a narrow range in M_{SMBH} exhibit this behavior of nearly constant N V / C IV, while the composites created from a narrow range in L do not (see Fig. 9). The composites at nearly constant L show a trend for increasing N V / C IV toward lower L/L_{Edd} (higher SMBH masses). The differences in emission-line behaviors at nearly constant M_{SMBH} and at nearly constant L have implications for the origin of the

Baldwin Effect (see Warner, Hamann, & Dietrich 2004, in prep). Throughout the rest of this manuscript (including figures and tables), “ L/L_{edd} composites” refer to the composite spectra created from our entire sample and sorted by L/L_{edd} .

4.4. Metallicities

We compare emission line flux ratios to plots of metallicity vs. line ratio based on theoretical models (see Figure 5 in Hamann et al. 2002 and Figure 3 in Warner et al. 2002). Ratios involving nitrogen lines are especially valuable in estimating metallicity, Z , due to the expected “secondary” N production via the CNO cycle of nucleosynthesis in stars (Shields 1976; Hamann & Ferland 1992, 1993, 1999; Ferland et al. 1996; Hamann et al. 2002). In the CNO cycle, N is produced from existing carbon and oxygen and thus the nitrogen abundance scales as $N/H \propto Z^2$ and $N/O \propto O/H \propto Z$ (Tinsley 1980), providing a sensitive metallicity diagnostic even when direct measurements of Z are not available (for more discussion, see Wheeler et al. 1989; Hamann & Ferland 1999; Henry et al. 2000; Hamann et al. 2003; Pilyugin 2003; Pilyugin et al. 2003). We prefer to base our metallicity estimates on the calculations in Hamann et al. (2002) that use a segmented powerlaw for the photoionizing continuum shape because this shape is a good approximation to the average observed continuum in quasars (Zheng et al. 1997; Laor et al. 1997) and it yields intermediate results for line ratios that are sensitive to the continuum shape, such as N V/He II.

Figure 10 shows metallicities inferred from several line ratios as a function of L/L_{edd} . The uncertainties shown in Figure 10 derive solely from the 1σ measurement uncertainties discussed in §3 and do not include the theoretical uncertainties in the technique we use to derive metallicities from the line ratios. Our best estimate of the overall metallicity from each spectrum (labeled as Average in Figure 10) is obtained by averaging the results of the line ratios that we believe are most accurately measured and most reliable from a theoretical viewpoint. Specifically, we average the metallicities derived from N III]/C III], N III]/O III], and N V/C IV (or when available, N V/(C IV+O VI)). See Hamann et al. (2002) and Warner et al. (2003) for further discussion.

All of the line ratios involving N III] and N V show N/O and N/C ratios that are solar or greater. This implies a metallicity of $\gtrsim 1 Z_{\odot}$ if N is mostly secondary. One implication of the unusual emission-line behavior with L/L_{edd} (discussed in §4.3) is that the derived metallicities on average show no trend with L/L_{edd} . The only line ratio to exhibit a strong trend with L/L_{edd} is N V/O VI.

Figure 11 shows our best estimates of the overall metallicities (derived from several line ratios, as described above for the “Average” in Figure 10) from the composite spectra sorted by L/L_{edd} , SMBH mass, and luminosity. The NLS1 composite spectrum is plotted in all three panels for comparison. The NLS1s exhibit a metallicity that is slightly high (a 30%–40% enhancement) for their SMBH masses and luminosities (see also Shemmer & Netzer 2002; Shemmer et al. 2003), but still well below the metallicities derived for most luminous quasars.

It is difficult to compare our results directly to Shemmer & Netzer (2002) because they measure only N V/C IV and

N V/He II ratios for a sample of individual objects. However, it does appear that the metallicity enhancement we derive as an average from several line ratios is smaller than the Shemmer & Netzer result based only on N V/C IV and N V/He II.

5. DISCUSSION

There is evidence supporting super-Eddington accretion rates for $\sim 27\%$ of the objects shown in Figures 1 and 4. Previous studies have also found quasars that appear to be accreting at super-Eddington rates (e.g., Collin et al. 2002, Vestergaard 2004). It is also worth noting that changing the index on the $R_{\text{BLR}} - L$ relationship (see §1) from 0.7 to 0.5 (e.g. Netzer & Laor 1993; Shields et al. 2003) would actually increase our estimates of L/L_{edd} , by as much as a factor of ~ 4 in the brightest quasars (see also Netzer 2003). Super-Eddington accretion can be explained simply by non-spherically symmetric accretion (Osterbrock 1989). It has been suggested that accretion disks with radiation-driven inhomogeneities could produce luminosities up to 100 times Eddington (Begelman 2002; Wang 2003).

Woo & Urry (2002) find that only 9% of their objects (21 out of 234, see their Fig. 7) have $L/L_{\text{edd}} > 1$. However, this may be due to the selection effect that their sample contains only 9 objects with $L > 10^{47}$ ergs s^{-1} . In our sample, only 13% of the objects with $L \leq 10^{47}$ ergs s^{-1} have $L/L_{\text{edd}} > 1$ (compared to 8%, 18 out of 225, in Woo & Urry 2002), but 41% of the objects in our sample with $L > 10^{47}$ ergs s^{-1} have super-Eddington ratios.

The NLS1 composite spectrum exhibits many properties unlike the L/L_{edd} composite spectra. The NLS1 composite has a much steeper (“softer”) UV continuum than the L/L_{edd} composites, consistent with studies finding that NLS1s generally have redder UV continua than typical AGNs (e.g., Crenshaw et al. 2002; Constantin & Shields 2003). There is no apparent trend between continuum shape and L/L_{edd} (Table 1), but there are trends between continuum shape and both SMBH mass (see Table 1; Warner et al. 2003) and luminosity (Table 1; M. Dietrich, private comm.), such that objects with lower SMBH masses and lower luminosities have steeper (“softer”) UV continua. Therefore, the steeper UV continuum in the NLS1 composite may be due to the NLS1 composite having a much lower average M_{SMBH} and L than the L/L_{edd} composites.

Interestingly, Figure 2 shows that the NLS1 composite spectrum most strongly resembles the composite spectrum created from objects with $L/L_{\text{edd}} > 2$. It seems to fit at the top of Figure 2 and not where it would be placed based on its average L/L_{edd} of 0.67. Based on this similarity between NLS1s and quasars with high L/L_{edd} , it has been suggested that high-redshift ($z \gtrsim 4$), high-luminosity, narrow-lined quasars are analogs of NLS1s (Mathur 2000). However, despite the similarity in Figure 2 between the NLS1 composite and the $L/L_{\text{edd}} > 2$ composite, the REWs of some emission lines in the two spectra can be quite different (see Figure 7, Constantin & Shields 2002). Moreover, the NLS1s do not fit the general trends in Figure 7 between emission line REW and L/L_{edd} .

If host galaxy mass, which correlates strongly with SMBH mass (see §1), is the fundamental parameter af-

fecting BLR metallicity, it is reasonable to expect no trend between metallicity and L/L_{edd} because there is no trend between L/L_{edd} and SMBH mass in the L/L_{edd} composites. The results in Figures 10 and 11 confirm this expectation. The different L/L_{edd} composites have similar average SMBH masses (Table 1) and similar metallicities. However, the NLS1 behavior is surprising. They have roughly the same metallicity as the L/L_{edd} composites even though their average SMBH mass and luminosity are almost two orders of magnitude lower. Figure 11 shows more directly that the NLS1s have slightly high metallicities for their luminosities and SMBH masses (see also Shemmer & Netzer 2002; Shemmer et al. 2003). If host galaxy mass, correlated with M_{SMBH} , is the main driver behind AGN metallicities (Figure 11 and Warner et al. 2003), then clearly some other factor is enhancing the metallicities in NLS1s. The magnitude of the NLS1 enhancement is modest, roughly 30%–40%. Note, in particular, that the NLS1 metallicities are still well below the values derived for most luminous (e.g., high-redshift) quasars.

Shemmer & Netzer (2002) suggest that high L/L_{edd} is driving the high metallicities in NLS1s. However, we have shown that there is no correlation between metallicity and L/L_{edd} (Figures 10 and 11). In addition, luminous narrow-lined quasars with the highest values of L/L_{edd} (such as BR2248-1242, Warner et al. 2002) do *not* have high metallicities for their SMBH masses. We conclude that the additional parameter affecting NLS1 metallicities is not related to L/L_{edd} .

Constantin & Shields (2003) suggest that the result for NLS1s having lower metallicities than high-redshift quasars runs counter to the hypothesis that these two groups of objects are in a similar early evolutionary phase. However, because the high-redshift quasars have higher SMBH masses and luminosities than NLS1s, they would naturally be expected to have higher metallicities. If both types of objects are in similar early evolutionary phases, and/or reside in young or rejuvenated host galaxies and the metallicities of both types of objects are thus enhanced by a similar amount, then the high-redshift quasars would still exhibit a higher metallicity than the NLS1s due to their higher SMBH masses. Thus, we conclude that more information is necessary to determine if either NLS1s or the high-redshift quasars (or both) are preferentially young objects.

6. SUMMARY & CONCLUSIONS

We have examined a large sample of 578 AGNs that spans five orders of magnitude in SMBH mass, seven orders of magnitude in luminosity, and a redshift range from $0 \leq z \leq 5$. We estimate SMBH masses using the virial theorem and formulae given in Kaspi et al. (2000), and then derive Eddington ratios. To improve the signal-to-noise ratio and average over object-to-object variations, we calculate composite spectra for different ranges in L/L_{edd} .

We include a composite spectrum of a sample of 26 NLS1s for comparative analysis. Our main results are as follows.

1) We find that a large fraction (27%) of the objects in our sample have $L/L_{\text{edd}} > 1$. These super-Eddington ratios may be explained by non-spherically symmetric accretion. While NLS1s generally show high Eddington ratios for their luminosities, the objects with the highest L/L_{edd} are high-luminosity, narrow-lined quasars.

2) There is no trend between L/L_{edd} and either redshift or SMBH mass. L/L_{edd} does correlate positively with luminosity and negatively with FWHM(C IV), but these trends may be attributed largely to our derivation of L/L_{edd} from these quantities (see Equation 4).

3) There is no trend between the shape of the UV continuum and L/L_{edd} . The NLS1 composite has a much steeper (softer) continuum than the L/L_{edd} composites. This is consistent with a trend between continuum shape and SMBH mass.

4) The composite spectra sorted by L/L_{edd} exhibit an unusual emission-line behavior: nearly constant peak heights and decreasing FWHMs with increasing L/L_{edd} (Figure 2). The origins of this behavior are not understood, but it is in marked contrast to the emission-line behaviors in composite spectra sorted by luminosity, SMBH mass, and FWHM(C IV) (Figure 8), all of which clearly show trends in the line REWs analogous to the Baldwin Effect.

5) The composite spectra show no trend between L/L_{edd} and metallicity (Figure 10). This is consistent with SMBH mass being related to the fundamental parameter affecting BLR metallicity (Warner et al. 2003).

6) The NLS1 composite exhibits several unusual behaviors. It generally does not fit the trends between emission line REWs and L/L_{edd} as defined by the L/L_{edd} composites. It also has a metallicity that is slightly high for its average SMBH mass and luminosity, although still well below the high metallicities exhibited by the most luminous quasars with the most massive central SMBHs. The quasars with the highest L/L_{edd} , high-luminosity quasars with narrow C IV emission, do not have high metallicities for their SMBH masses and luminosities. Our earlier work (Warner et al. 2003) is consistent with the theory that host galaxy mass, correlated with SMBH mass (and AGN luminosity), is the fundamental parameter affecting BLR metallicity. We conclude that i) there must be some secondary effect enhancing the metallicity in NLS1s, and ii) this secondary effect is not related to L/L_{edd} .

Acknowledgements: We are very grateful to Marianne Vestergaard for providing the UV Fe emission template for this study, and to Fred Chaffee, Anca Constantin, Craig Foltz, Vesa Junkkarinen, and Joe Shields for their direct participation in reducing or acquiring some of the ground-based spectra. We acknowledge financial support from the NSF via grant AST99-84040 and NASA via grant NAG5-3234.

REFERENCES

- Begelman, M. C. 2002, ApJ, 568, L97
 Bettoni, D., Falomo, R., Fasanò, G., & Govoni, F. 2003, A&A, 399, 869
 Bischof, O. B. & Becker, R. H. 1997, AJ, 113, 2000
 Boroson, T. A. 2002, ApJ, 565, 78
 Boroson, T. A. 2003, ApJ, 585, 647
 Boroson, T. A. & Green, R. F. 1992, ApJS, 80, 109
 Brotherton, M. S. et al. 2001, ApJ, 546, 775
 Carroll, S. M., Press, W. H., & Turner, E. L. 1992, ARA&A, 30, 499
 Collin, S. et al. 2002, A&A, 388, 771

- Constantin, A. & Shields, J. C. 2003, *PASP*, 115, 592
 Corbett, E. A. et al. 2003, *MNRAS*, 343, 705
 Crenshaw, D. M. et al. 2002, *ApJ*, 566, 187
 Croom, S. M. et al. 2002, *MNRAS*, 337, 275
 Dietrich, M. et al. 1999, *A&A*, 352, L1
 Dietrich, M., Hamann, F. et al. 2002, *ApJ*, 581, 912
 Elvis, M. et al. 1994, *ApJS*, 95, 1
 Erwin, P., Graham, A. W., & Caon, N. 2002, *astro-ph/0212335*
 Ferland, G. J. et al. 1996, *ApJ*, 461, 683
 Ferrarese, L. & Merritt, D. 2000, *ApJ*, 539, L9
 Gebhardt, K. et al. 2000, *ApJ*, 539, L13
 Graham, A. W., Erwin, P., Caon, N., & Trujillo, I. 2001, *ApJ*, 563, L11
 Hamann, F. & Ferland, G. 1992, *ApJ*, 391, L53
 Hamann, F. & Ferland, G. 1993, *ApJ*, 418, 11
 Hamann, F., Shields, J. C., Burbridge, E. M., Junkkarinen, V., & Crenshaw, D. M. 1998, *ApJ*, 496, 761
 Hamann, F. & Ferland, G. 1999, *ARA&A*, 37, 487
 Hamann, F., Korista, K. T., Ferland, G. J., Warner, C., & Baldwin, J. 2002, *ApJ*, 564, 592
 Hamann, F., Dietrich, M., Sabra, B., & Warner, C. 2003, *astro-ph/0306068*
 Henry, R. B. C., Edmunds, M. G., & Köppen, J. 2000, *ApJ*, 541, 660
 Kaspi, S., Smith, P. S., Netzer, H., Maoz, D., Jannuzi, B. T., & Giveon, U. 2000, *ApJ*, 533, 631
 Kellermann, K. I. et al. 1989, *AJ*, 98, 1195
 Korista, K.T. et al. 1995, *ApJS*, 97, 285
 Krolik, J. 2001, *ApJ*, 551, 72
 Kuraszewicz, J., Wilkes, B., Czerny, B., & Mathur, S. 2000, *ApJ*, 542, 692
 Laor, A., Jannuzi, B. T., Green, R. F., & Boroson, T. A. 1997, *ApJ*, 489, 656
 Laor, A. 1998, *ApJ*, 505, L83
 Magorrian, J. et al. 1998, *AJ*, 115, 2285
 Mathur, S. 2000, *MNRAS*, 314, 17
 McLure, R. J. & Dunlop, J. S. 2001, *MNRAS*, 327, 199
 McLure, R. J. & Dunlop, J. S. 2002, *MNRAS*, 331, 795
 McLure, R. J. & Jarvis, M. J. 2002, *MNRAS*, 337, 109
 Merritt, D. & Ferrarese, L. 2001, *ApJ*, 547, 140
 Nelson, C. H. 2000, *ApJ*, 544, L91
 Netzer, H. & Laor, A. 1993, *ApJ*, 404, L51
 Netzer, H. 2003, *ApJ*, 583, L5
 Osterbrock, D. E. 1989, *Astrophysics of Gaseous Nebulae and Active Galactic Nuclei* (Sausalito, California: University Science Books)
 Osterbrock, D. E. & Pogge, R. W. 1985, *ApJ*, 297, 166
 Peterson, B. M. 1993, *PASP*, 105, 247
 Peterson, B. M. 1997, *An Introduction to Active Galactic Nuclei* (Cambridge: Cambridge University Press)
 Peterson, B. M. & Wandel, A. 1999, *ApJ*, 521, L95
 Peterson, B. M. & Wandel, A. 2000, *ApJ*, 540, L13
 Pilyugin, L. S. 2003, *A&A*, 399, 1003
 Pilyugin, L. S., Thuan, T. X., & Vilchez, J. M. 2003, *A&A*, 397, 487
 Rees, M. J. 1984, *ARA&A*, 22, 471
 Shemmer, O. & Netzer, H. 2002, *ApJ*, 567, L19
 Shemmer, O. et al. 2003, in *ASP Conf. Ser.* in press, *AGN Physics with the Sloan Digital Sky Survey*, ed. G. T. Richards & P. B. Hall
 Shields, G. A. 1976, *ApJ*, 204, 330
 Shields, G. A. et al. 2003, *ApJ*, 583, 124
 Steidel, C. C. et al. 2002, *ApJ*, 576, 653
 Stern, D. et al. 2000, *AJ*, 119, 1526
 Stirpe, G. M. et al. 1994, *ApJ*, 425, 609
 Tremaine, S. et al. 2002, *ApJ*, 574, 740
 Tinsley, B. 1980, *Fundam. Cosmic Physics*, 5, 287
 Vanden Berk, D. E. et al. 2001, *AJ*, 122, 549
 Véron-Cetty, M.-P. & Véron, P. 2001, "A Catalogue of Quasars and Active Nuclei", 10th edition
 Vestergaard, M. & Wilkes, B. J. 2001, *ApJS*, 134, 1
 Vestergaard, M. 2002, *ApJ*, 571, 733
 Vestergaard, M. 2004, *ApJ*, in press
 Wandel, A. 1999, *ApJ*, 519, L39
 Wandel, A., Peterson, B. M., & Malkan, M. A. 1999, *ApJ*, 526, 579
 Wang, T. & Lu, Y. 2001, *A&A*, 377, 52
 Wang, J.-M. 2003, *AJ*, 125, 2859
 Warner, C., Hamann, F., Shields, J. C., Constantin, A., Foltz, C., & Chaffee, F. 2002, *ApJ*, 567, 68
 Warner, C., Hamann, F., & Dietrich, M. 2003, *ApJ*, 596, 72
 Wheeler, J. C., Sneden, C., & Truran, J. W. 1989, *ARA&A*, 27, 279
 Wills, B. J., Brotherton, M. S., Fang, D., Steidel, C. C., & Sargent, W. L. W. 1993, *ApJ*, 415, 563
 Wills, B. J. et al. 1995, *ApJ*, 447, 139
 Wilkes, B. J. et al. 1999, *ApJ*, 513, 76
 Zheng, W., Kriss, G. A., Telfer, R. C., Grimes, J. P., & Davidsen, A. F. 1997, *ApJ*, 475, 469

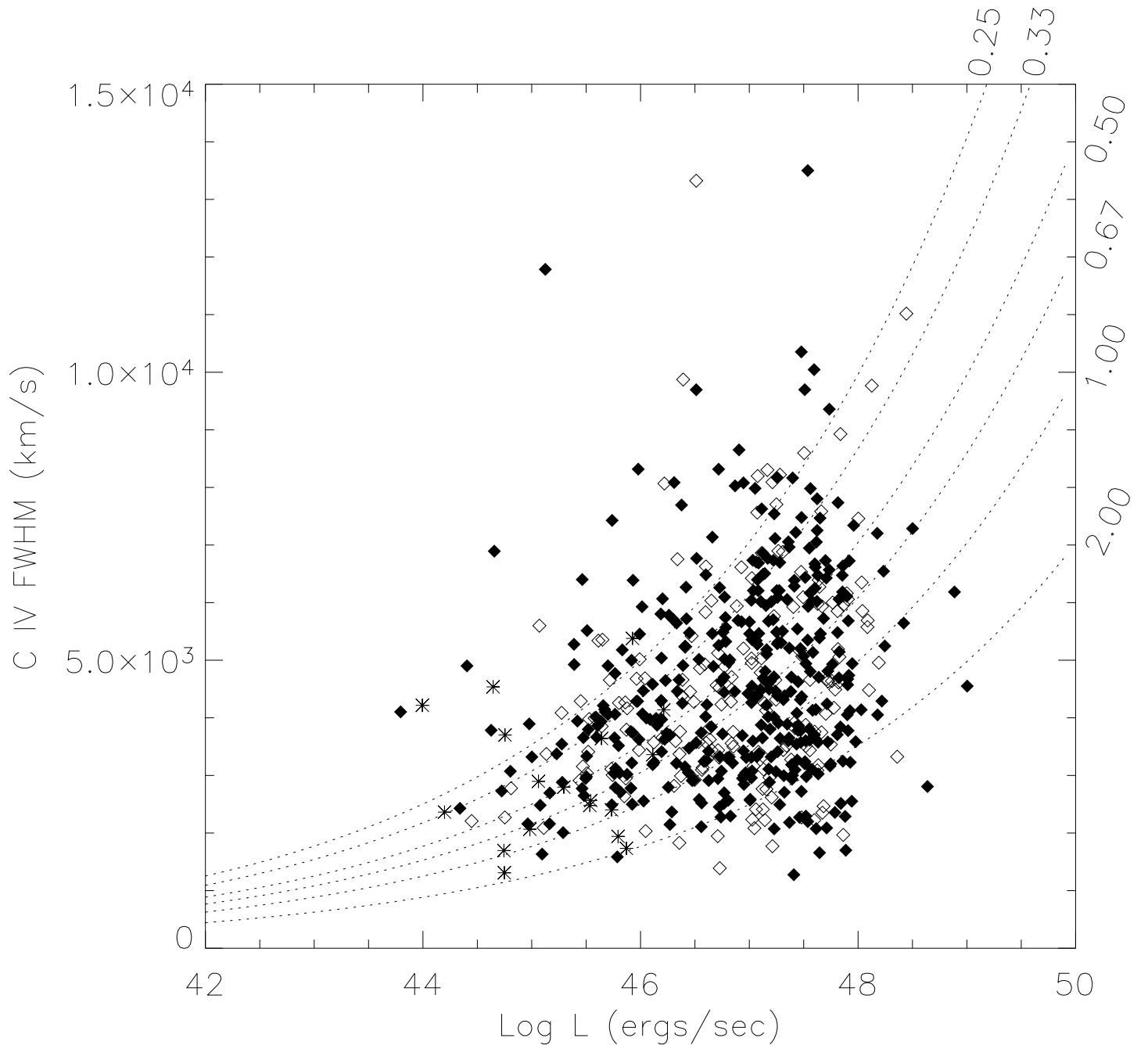


FIG. 1.— Distribution of the two measured quantities. The dotted lines represent constant L/L_{edd} ratios, with values indicated at the right. We created composite spectra for each of the seven ranges in Eddington ratio shown above. The filled diamonds represent radio-quiet quasars, the open diamonds represent radio-loud quasars, and the asterisks represent NLS1s.

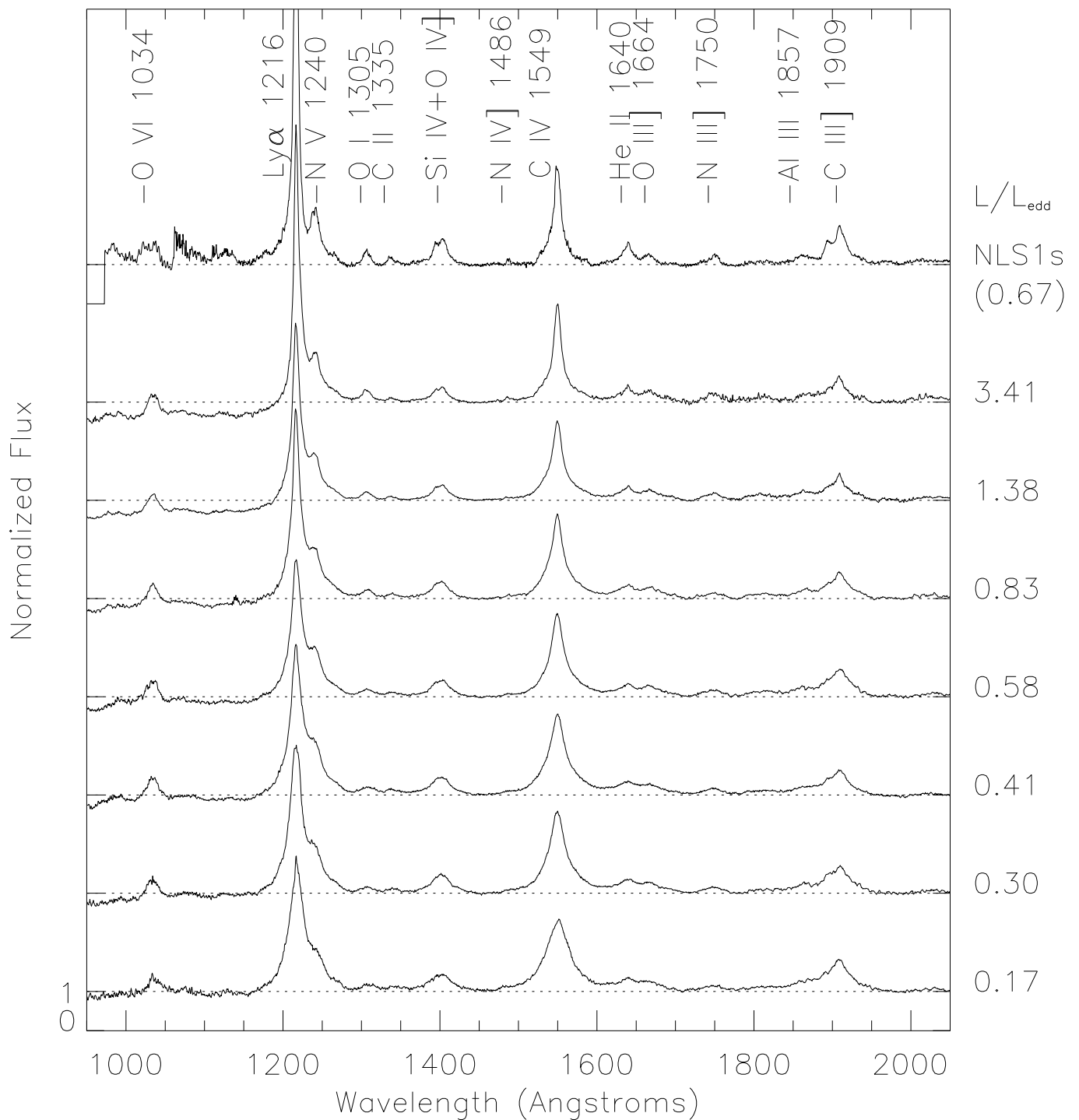


FIG. 2.— Composite spectra, sorted by L/L_{edd} , with the mean L/L_{edd} values indicated at the right. The top spectrum is a composite spectrum created only from objects identified in the literature as NLS1s. The horizontal dashed lines and tick marks indicate the normalized continuum levels for each composite spectrum. The scaled height of the normalized continua above zero flux, as indicated for the bottom spectrum, is the same for all spectra plotted.

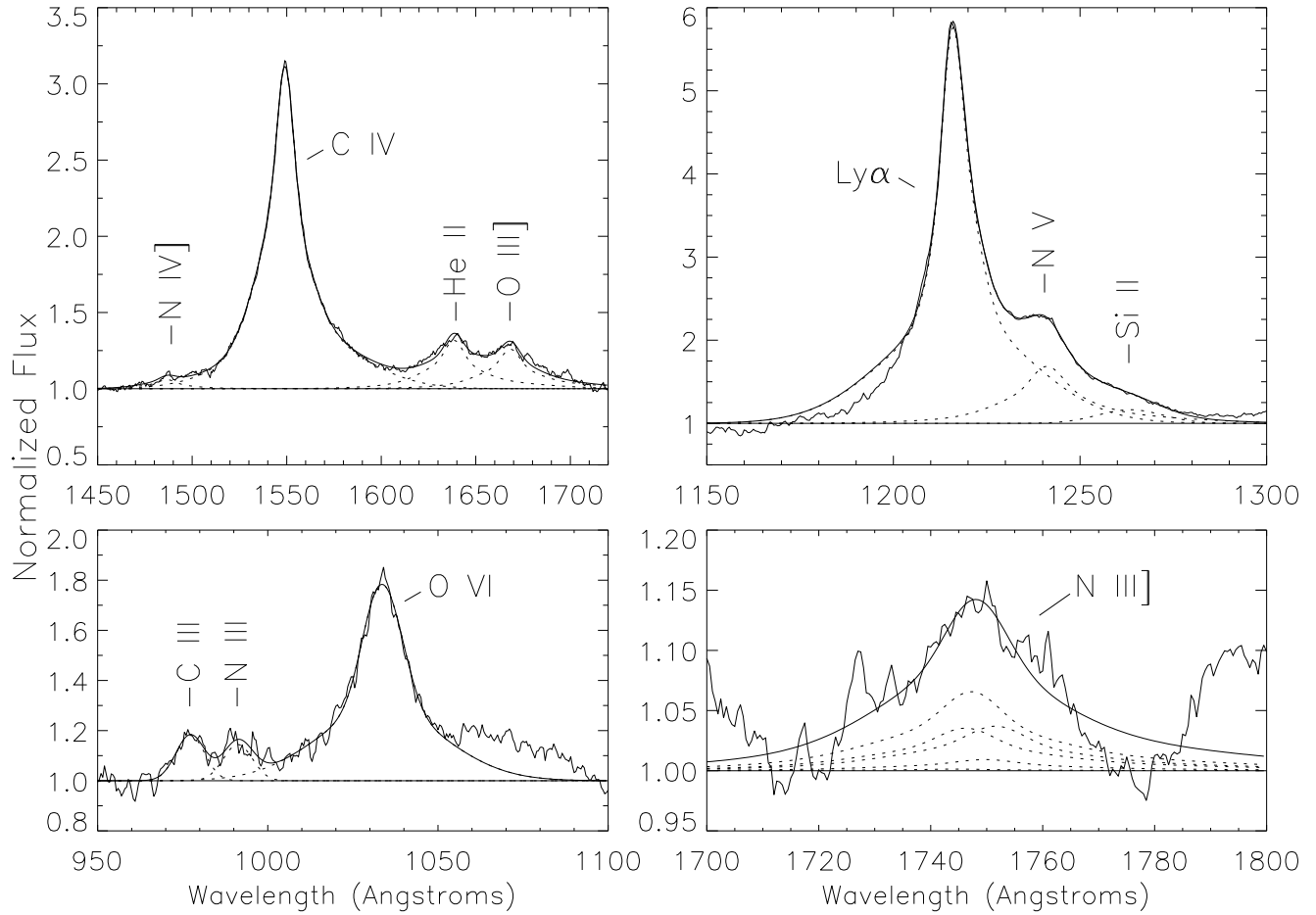


FIG. 3.— Multi-component Gaussian fits (smooth solid curves) to observed emission lines (jagged solid curves) for a composite spectrum of $\langle L/L_{edd} \rangle \sim 0.58$. The continuum is normalized by a power law continuum fit. The continuum (at unity) and composite line fits are plotted. The individual components of the fits to N III] as dotted lines. In the other panels, the dotted lines represent the sum contribution of each labelled emission line. There is an unidentified bump at $\sim 1070 \text{ \AA}$ that is not attributed to O VI (see Hamann et al. 1998).

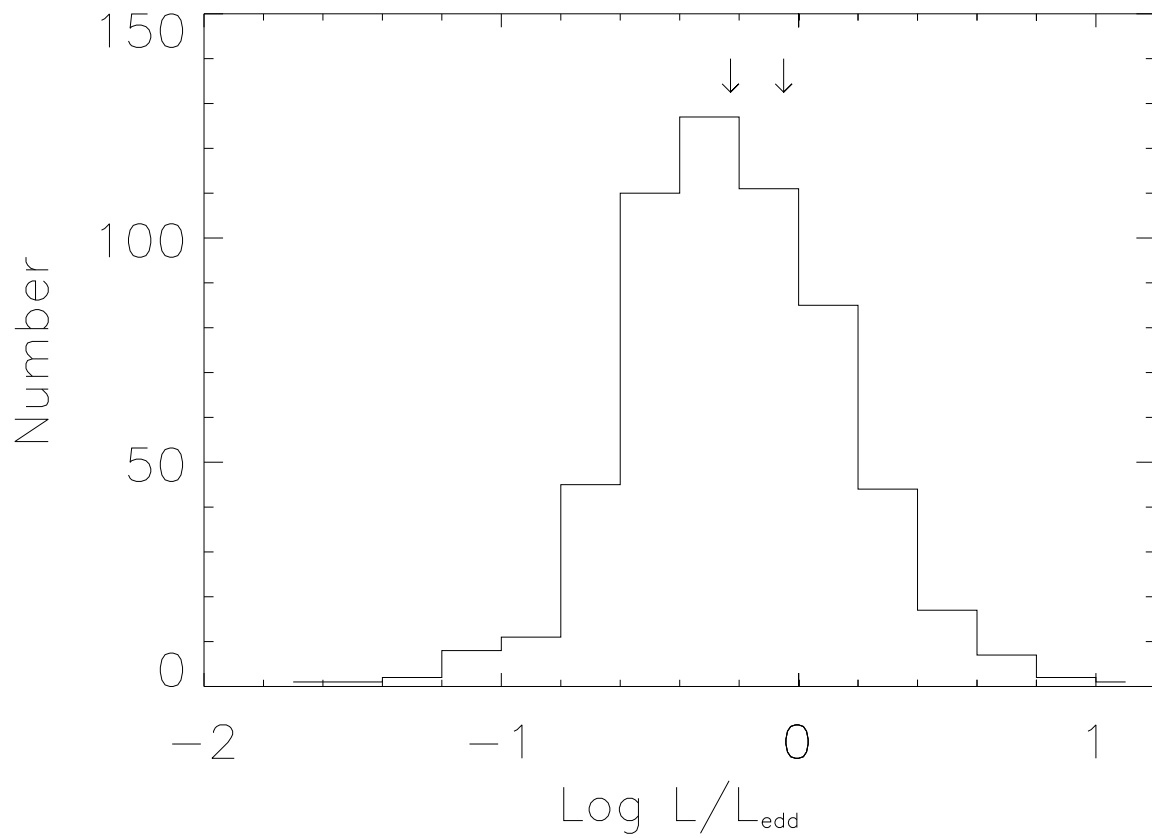


FIG. 4.— Distribution of estimated Eddington ratio, L/L_{edd} . The two arrows are the median (0.59) and mean (0.89) L/L_{edd} of the entire sample. About 27% of the objects have $L/L_{\text{edd}} > 1$.

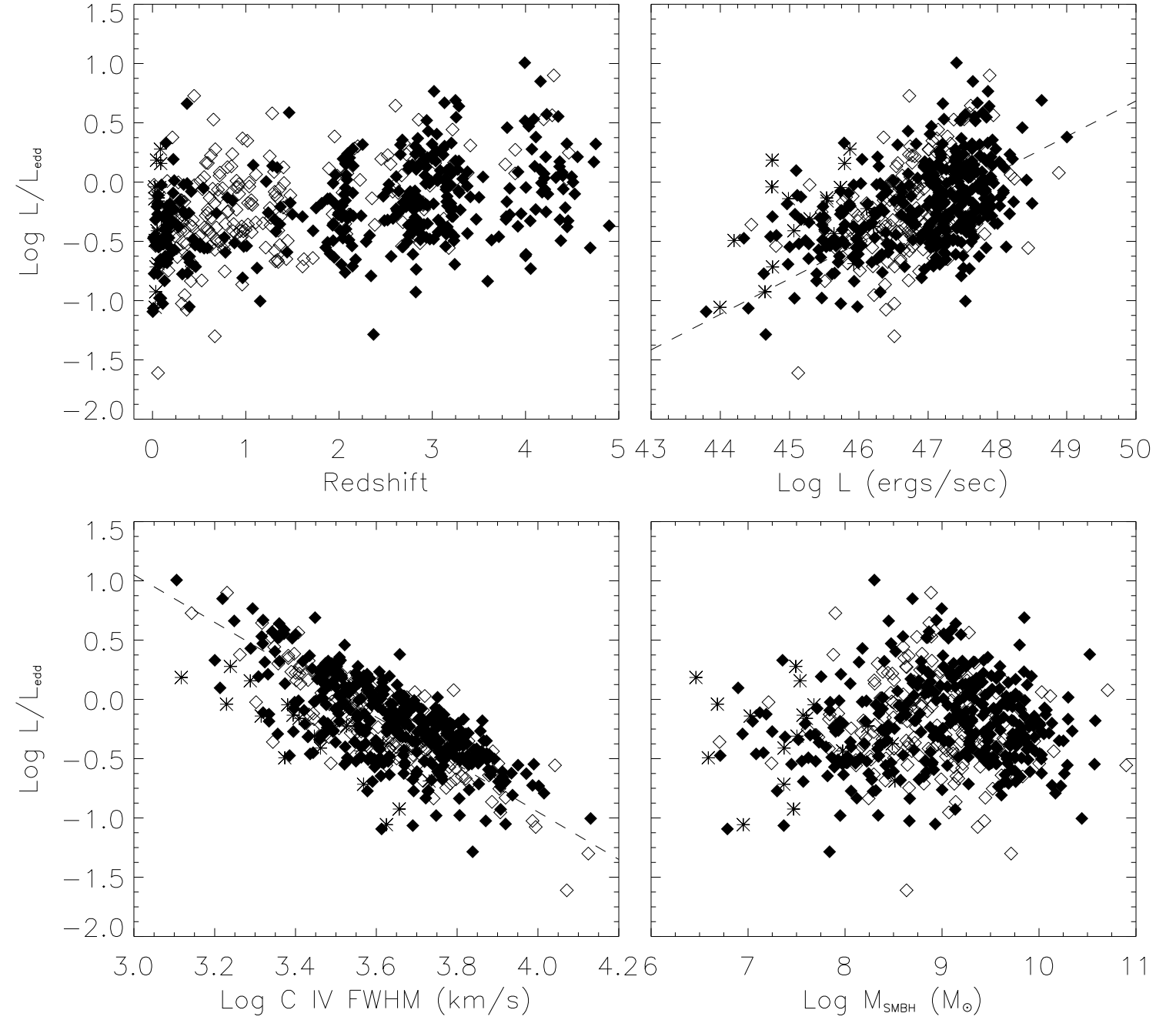


FIG. 5.— Symbols as in Fig. 1. The dashed lines represent slopes from the L/L_{edd} equation (not fits). The positive correlation with L and negative correlation with $\text{FWHM}(\text{C IV})$ may be attributed largely to our derivation of L/L_{edd} from these quantities (see Equation 4).

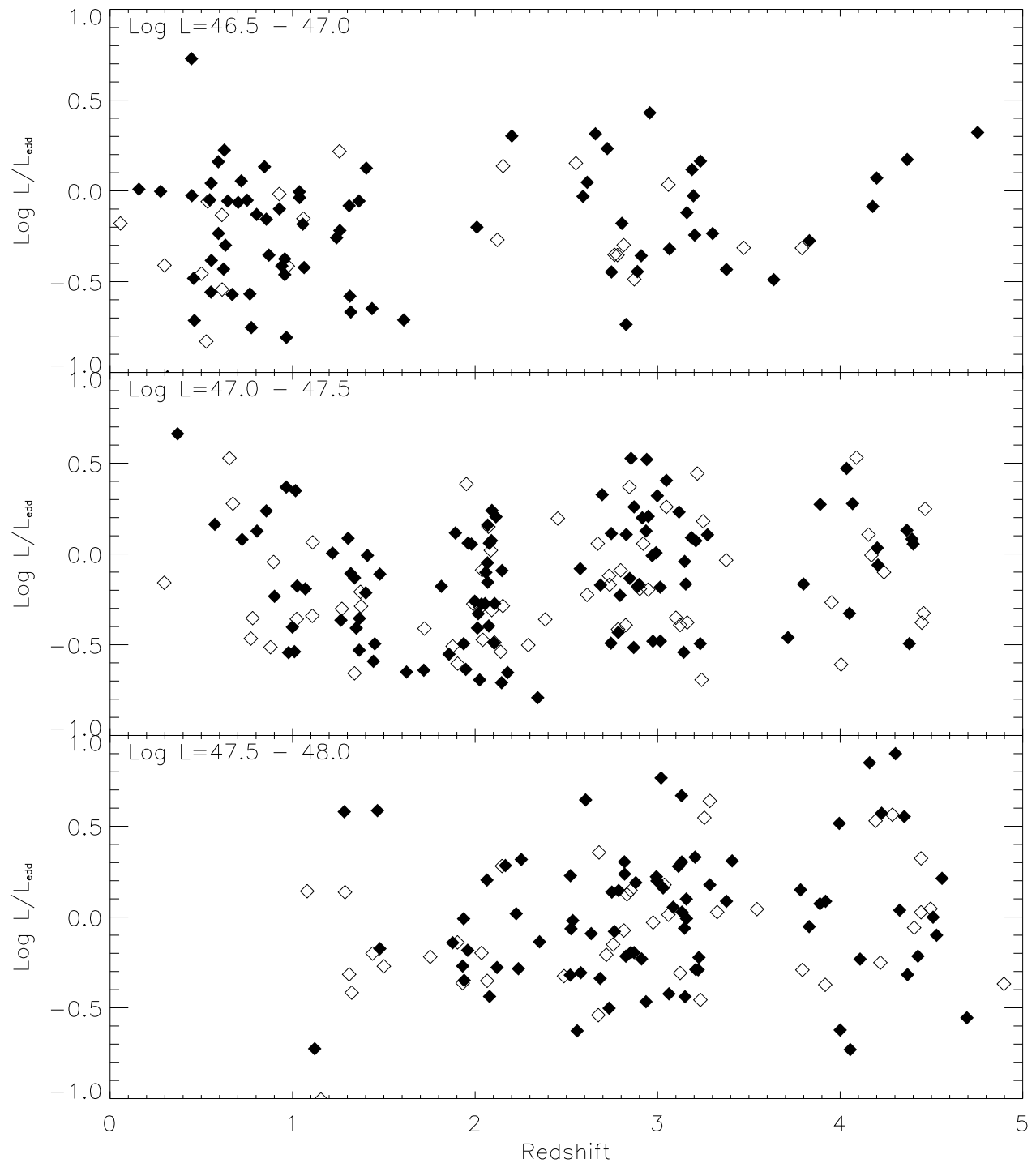


FIG. 6.— Symbols as in Fig. 1. In bins of narrow luminosity ranges, there is no apparent trend between L/L_{edd} and redshift. Our sample, though, does seem to have a selection effect for more higher luminosity objects at higher redshifts. This, combined with the trend for higher luminosity objects to have higher L/L_{edd} , explains the slight trend that seems to exist in Fig. 5 between L/L_{edd} and redshift.

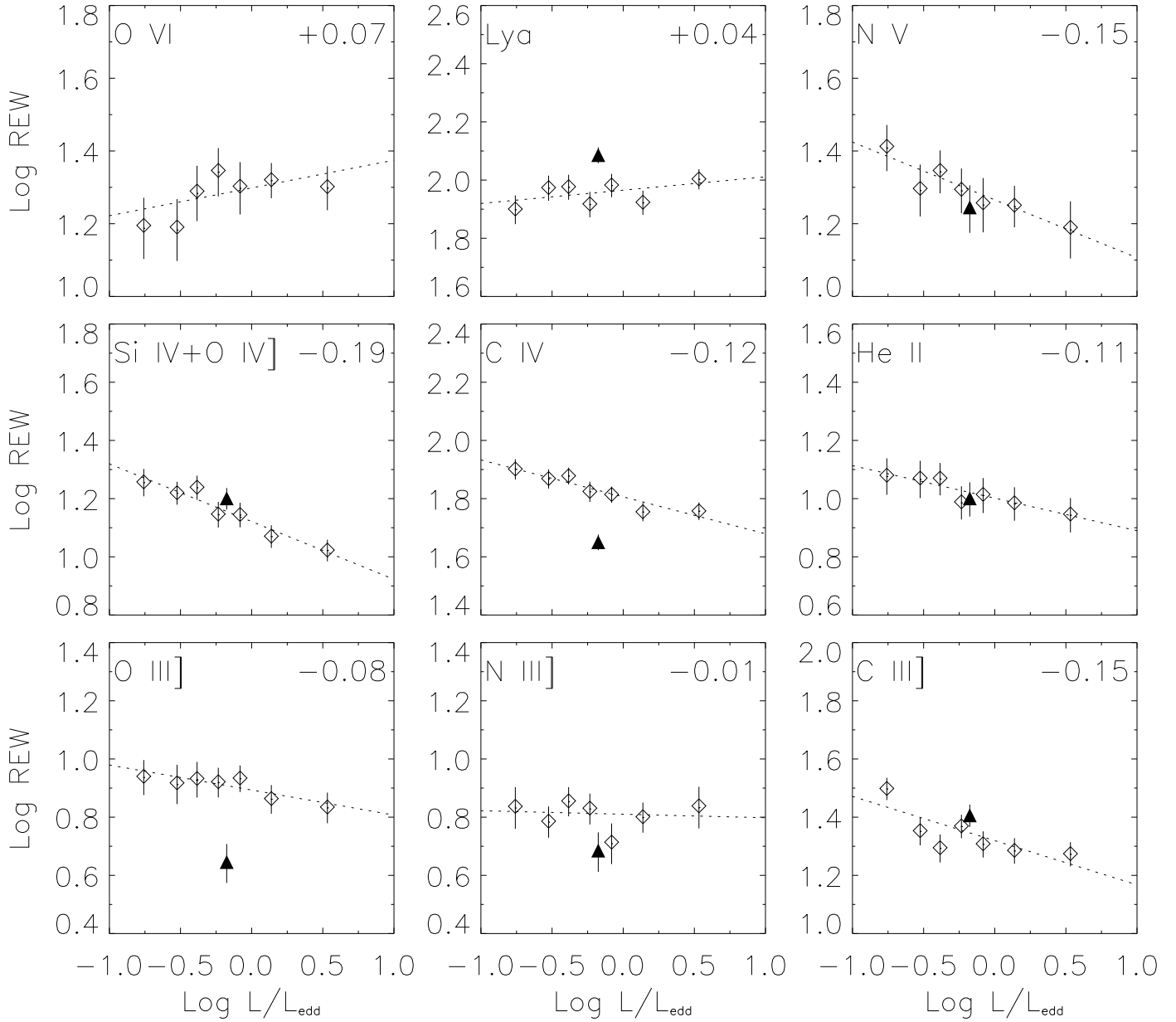


FIG. 7.— The diamonds represent the L/L_{edd} composites and the triangle represents the NLS1 composite. REWs are in angstroms. The dotted lines are linear fits to the L/L_{edd} composites, with slopes given in the upper right. The uncertainties shown are the 1σ standard deviations in the REWs based on repeated estimates with the continuum drawn at different levels (see §3).

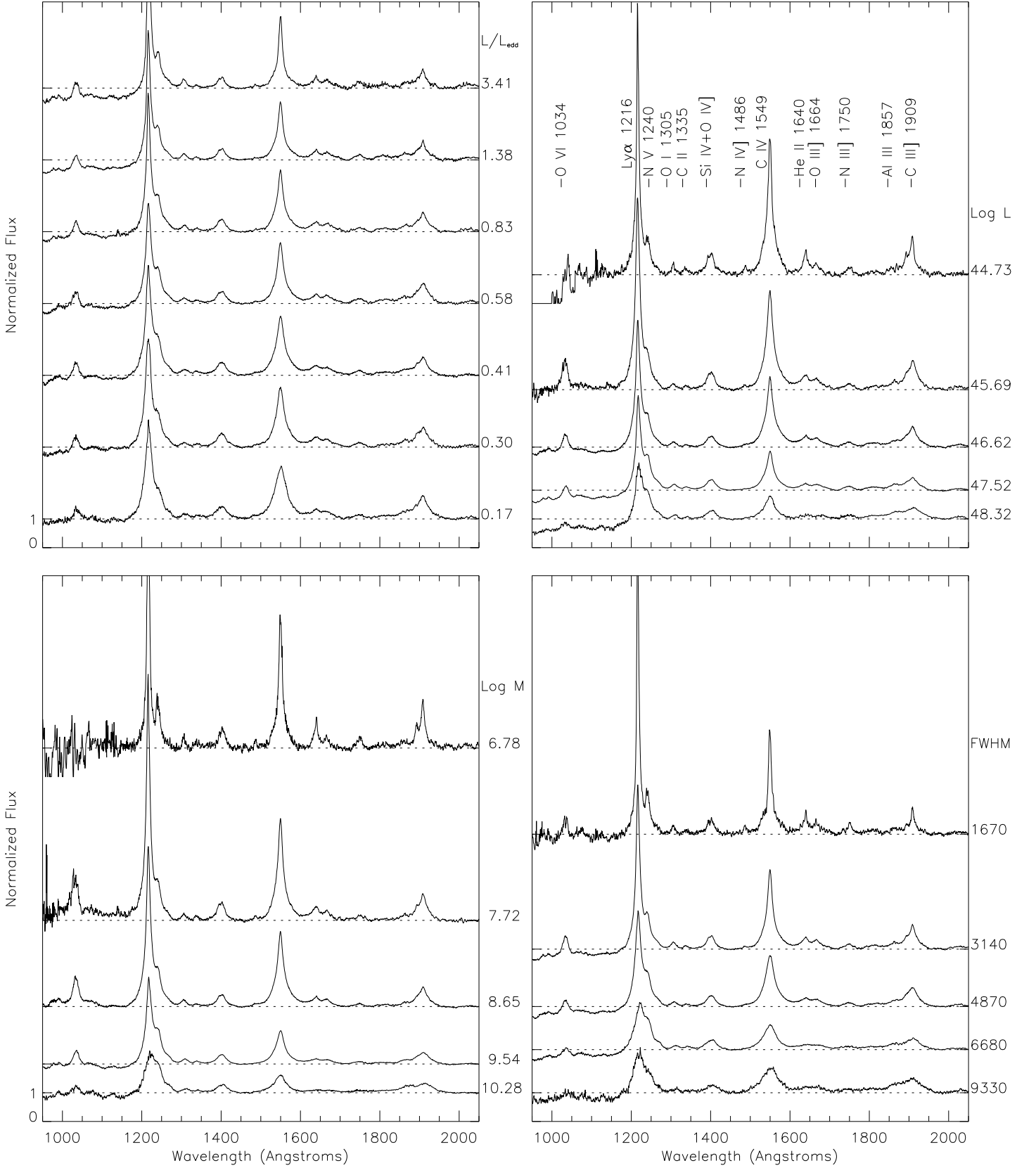


FIG. 8.— Normalized composite spectra sorted by L/L_{Edd} (top left, identical to Fig. 2 without the NLS1 composite) are compared to normalized composite spectra computed from different ranges in bolometric luminosity (top right, in units of ergs/sec), SMBH mass (bottom left, in M_{\odot}), and FWHM(C IV) (bottom right, in km/sec). Dashed lines and tick marks as in Fig. 2. The L , SMBH mass, and FWHM(C IV) composite spectra all clearly show trends for decreasing line equivalent widths and peak heights as luminosity, SMBH mass, and FWHM(C IV) increase. The composite spectra sorted by FWHM(C IV) even exhibit this trend despite spanning less than half an order of magnitude in average luminosity, a much narrower range than in the L/L_{Edd} composites (see Table 1). However, the L/L_{Edd} composites show nearly constant peak heights and decreasing FWHMs with increasing L/L_{Edd} .

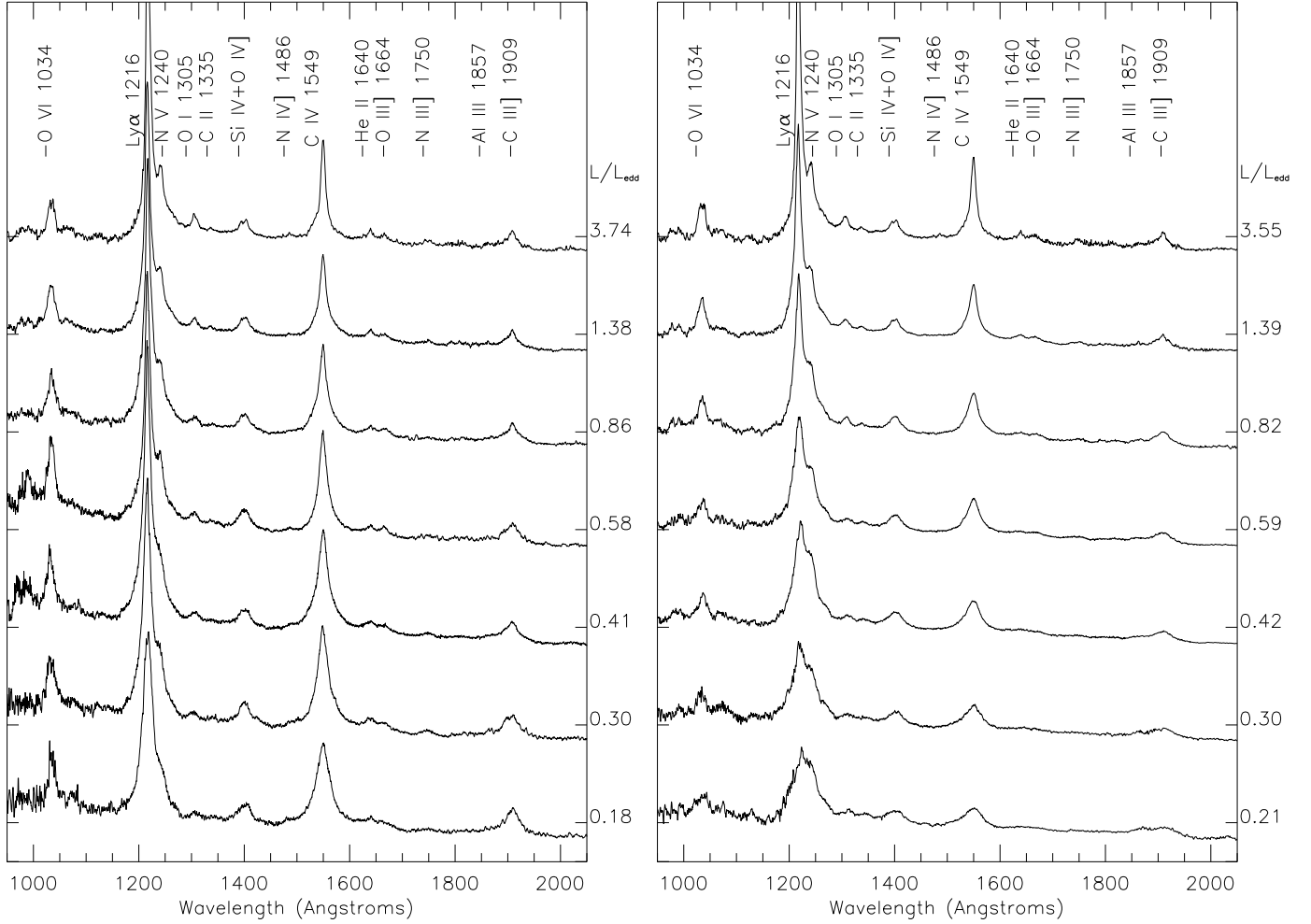


FIG. 9.— Composite spectra sorted by L/L_{edd} for a narrow range in SMBH mass of $10^8 M_{\odot} < M_{\text{SMBH}} < 10^9 M_{\odot}$ (left) are compared to ones sorted by L/L_{edd} for narrow range in luminosity of $10^{47} \text{ ergs/s} < L < 10^{48} \text{ ergs/s}$ (right). The spectra are shown prior to normalization to the continuum. The composite spectra at nearly constant M_{SMBH} show the same emission-line behavior as the L/L_{edd} composites created from our entire sample: nearly constant peak heights and decreasing FWHMs with increasing L/L_{edd} . In contrast, the composite spectra at nearly constant L do not share this behavior and show a trend similar to the Baldwin Effect: decreasing peak heights and equivalent widths with increasing M_{SMBH} .

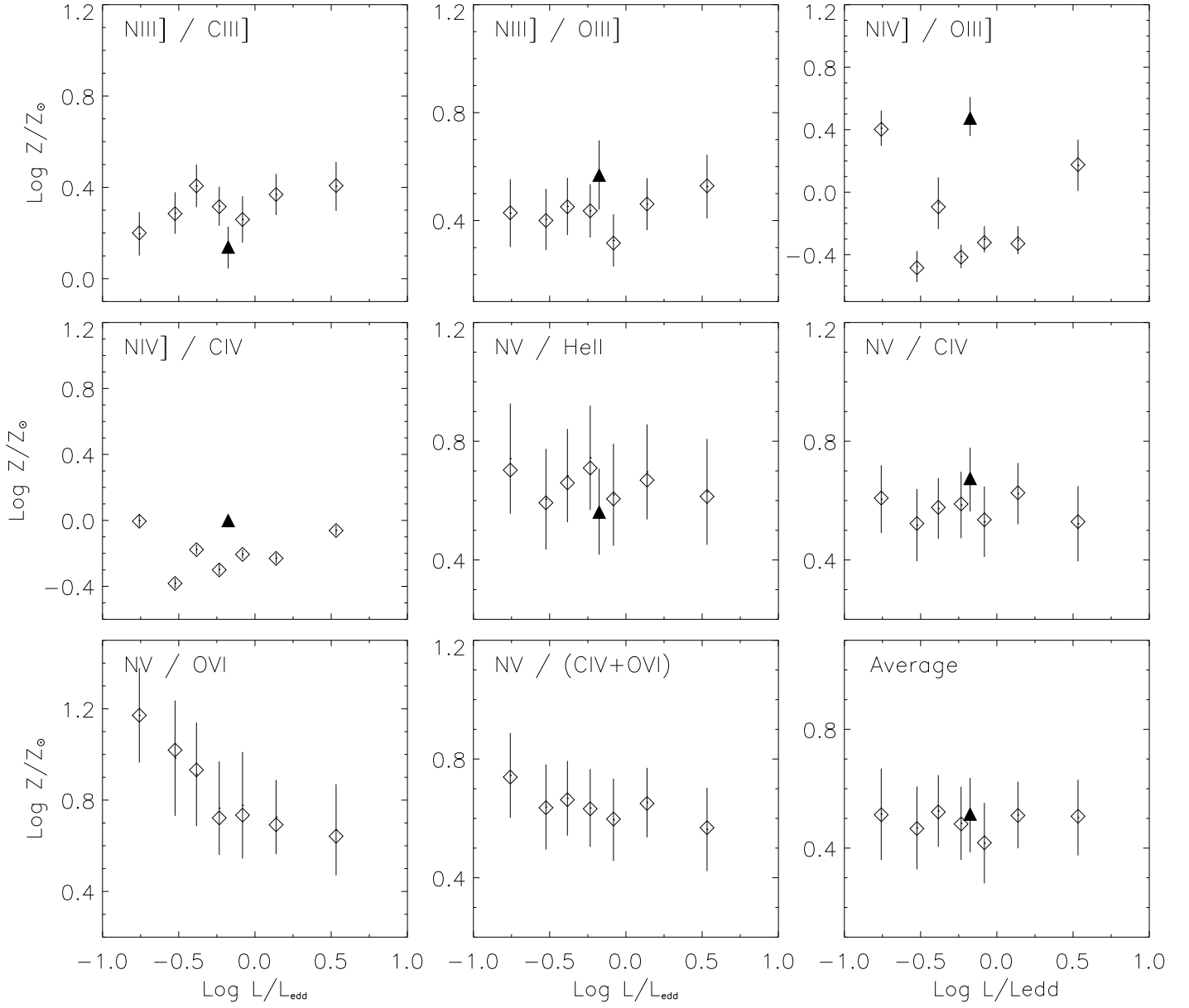


FIG. 10.— Metallicities derived from comparisons of different line ratio diagnostics to theoretical results from Figure 5 in Hamann et al. (2002) are shown as a function of L/L_{Edd} . The average includes N III]/C III] , N III]/O III] , and N V/(C IV+O VI) . Symbols as in Fig. 7.

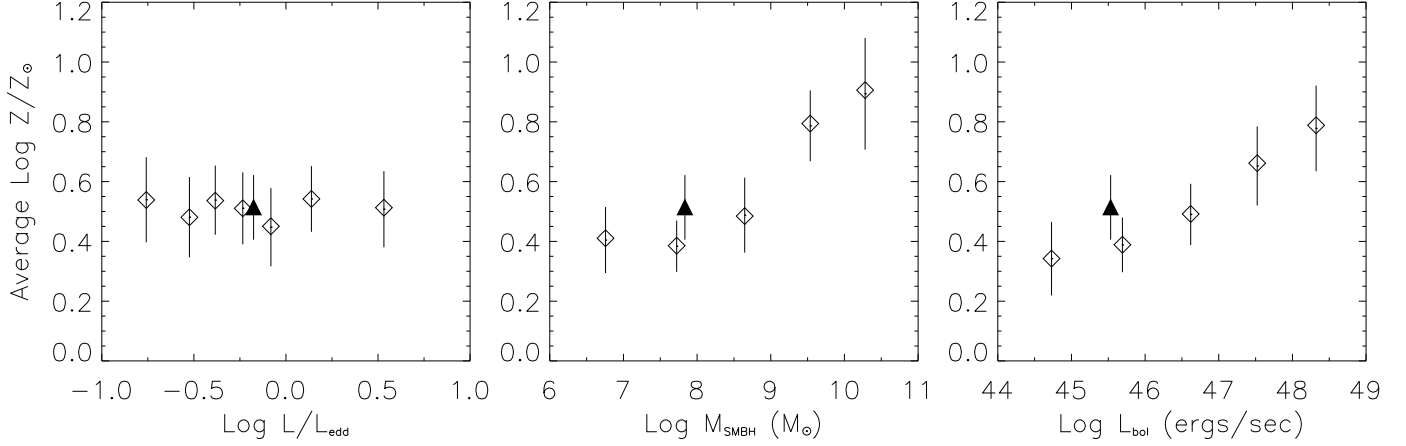


FIG. 11.— Symbols as in Fig. 7. Our best estimates of the overall metallicity of each spectrum are shown for the L/L_{edd} , SMBH mass, and luminosity composite spectra. The NLS1 composite, plotted in all three panels as a filled triangle, has a metallicity that is slightly high for its SMBH mass and luminosity, but still well below the metallicities of most luminous quasars.

TABLE 1
COMPOSITE PARAMETERS

L/L_{edd}	α	# Objects at C IV	z	Log L [ergs s ⁻¹]	FWHM(C IV) [km s ⁻¹]	Log M_{SMBH} [M _⊙]
————— L/L_{edd} Composites —————						
0.17	-0.65	64	1.06	46.84	6900	9.48
0.30	-0.56	62	1.17	47.17	5600	9.60
0.41	-0.49	106	1.62	47.16	5100	9.44
0.58	-0.40	85	1.83	47.43	4600	9.56
0.83	-0.60	90	1.93	47.37	3900	9.36
1.38	-0.33	110	2.55	47.63	3400	9.42
3.41	-0.54	45	2.86	47.84	2400	9.26
————— NLS1s —————						
0.67	-0.93	18	0.06	45.53	2900	7.83
————— L Composites —————						
0.43	-0.73	15	0.57	44.73	3100	7.25
0.46	-0.66	90	0.37	45.69	3800	8.10
0.69	-0.36	155	1.39	46.62	4400	8.87
1.15	-0.47	278	2.63	47.52	4900	9.59
1.21	-0.24	20	3.01	48.32	5900	10.30
————— M_{SMBH} Composites —————						
0.61	-0.98	7	0.56	44.62	2500	6.78
0.69	-0.90	61	0.46	45.68	3000	7.27
1.08	-0.71	198	1.43	46.84	3800	8.65
0.84	-0.59	261	2.46	47.52	5200	9.54
0.58	-0.57	34	2.84	48.17	7500	10.28
————— FWHM(C IV) Composites —————						
3.94	-0.91	14	1.64	47.25	1700	8.35
1.24	-0.48	237	1.71	47.22	3100	8.87
0.58	-0.38	195	1.86	47.48	4900	9.43
0.38	-0.42	91	2.29	47.65	6700	9.84
0.17	-0.47	25	1.89	47.52	9300	10.07

TABLE 2
EMISSION LINE DATA

L/L_{edd}	Property	O VI $\lambda 1034$	Ly α $\lambda 1216$	N V $\lambda 1240$	C IV $\lambda 1549$	He II $\lambda 1640$	O III] $\lambda 1665$	N III] $\lambda 1750$	C III] $\lambda 1909$
0.17	Flux/Ly α	0.21	1.00	0.32	0.75	0.10	0.07	0.06	0.22
	REW ^a	16	80	26	80	12	9	7	32
	FWHM ^b	5500	4700	6900	6800	6800	6800	6900	4900
0.30	Flux/Ly α	0.17	1.00	0.21	0.57	0.08	0.06	0.04	0.13
	REW ^a	16	94	20	74	12	8	6	23
	FWHM ^b	5200	4300	5100	4800	4800	4800	5000	5000
0.41	Flux/Ly α	0.21	1.00	0.23	0.57	0.08	0.06	0.05	0.11
	REW ^a	19	95	22	76	12	9	7	20
	FWHM ^b	6200	4600	5300	4900	4900	4900	5100	4300
0.58	Flux/Ly α	0.28	1.00	0.24	0.57	0.08	0.06	0.05	0.14
	REW ^a	22	83	20	67	10	8	7	23
	FWHM ^b	6500	3800	4300	4000	4000	4000	4200	4900
0.83	Flux/Ly α	0.22	1.000	0.19	0.50	0.07	0.06	0.03	0.12
	REW ^a	20	96	18	65	10	9	5	20
	FWHM ^b	5200	3000	4300	3700	3700	3700	4000	4000
1.38	Flux/Ly α	0.26	1.00	0.21	0.47	0.07	0.05	0.04	0.11
	REW ^a	21	84	18	57	10	7	6	19
	FWHM ^b	5500	2800	3900	3300	3300	3300	3600	3500
3.41	Flux/Ly α	0.21	1.00	0.15	0.41	0.06	0.04	0.04	0.10
	REW ^a	20	100	15	57	9	7	7	19
	FWHM ^b	5100	2100	3000	2500	2500	2500	2800	3100
0.67 (NLS1s)	Flux/Ly α	–	1.00	0.14	0.29	0.06	0.03	0.03	0.13
	REW ^a	–	122	18	45	10	4	5	25
	FWHM ^b	–	2100	2800	2200	2200	2200	2700	3100

^aIn units of \AA

^bIn units of km s^{-1}